

is 3 nm (29), which is consistent with the grain boundary widths (which correspond to atomic-scale features) seen in our plasmon energy maps (fig. S1). However, the sample does not support a temperature gradient for separations smaller than the electron mean free path ℓ_e because electrons are ballistic over distances less than ℓ_e . Thus, ℓ_e describes the smallest thermal feature size that can exist in continuous aluminum. Similarly, because phonons generate thermal expansion, temperature cannot produce different densities at separations smaller than a phonon mean free path ℓ_{ph} . We estimate $\ell_e \lesssim 4$ to 15 nm and $\ell_{ph} \lesssim 2$ to 5 nm in our temperature range (table S1). For Λ_{p1} smaller than ℓ_{ph} or ℓ_e , PEET achieves the maximum possible spatial resolution; temperature differences do not exist on length scales smaller than the larger mean free path.

PEET is applicable to many other technologically important metals and semiconductors. Tungsten, silver, silicon, gallium arsenide, and gallium nitride all have sufficiently sharp plasmon resonances (29). [The width of the plasmon resonance limits PEET's precision, so decreasing the zero loss peak width (30) gives only a small sensitivity improvement.] Because the product of the thermal expansion coefficient α with the melting temperature is $\alpha T_m \sim 0.02$ for many materials (31), one will generally trade high sensitivity for a large accessible temperature range, or vice versa, depending on the application. Ideally, the system to be measured serves as its own thermometer, without requiring the introduction of thermometric materials that might compromise the thermal behavior or device function.

REFERENCES AND NOTES

1. F. Reif, *Fundamentals of Statistical and Thermal Physics* (McGraw-Hill, New York, 1965).
2. M. Hartmann, G. Mahler, O. Hess, *Phys. Rev. Lett.* **93**, 080402 (2004).
3. Y. Dubi, M. Di Ventra, *Rev. Mod. Phys.* **83**, 131–155 (2011).
4. J. Christofferson *et al.*, *J. Electron. Packag.* **130**, 041101 (2008).
5. C. D. S. Brites *et al.*, *Nanoscale* **4**, 4799–4829 (2012).
6. S. B. Singer, M. Mecklenburg, E. R. White, B. C. Regan, *Phys. Rev. B* **84**, 195468 (2011).
7. V. V. Deshpande, S. Hsieh, A. W. Bushmaker, M. Bockrath, S. B. Cronin, *Phys. Rev. Lett.* **102**, 105501 (2009).
8. G. Tessier, M. Bardoux, C. Boué, C. Filloy, D. Fournier, *Appl. Phys. Lett.* **90**, 171112 (2007).
9. G. Kucsko *et al.*, *Nature* **500**, 54–58 (2013).
10. E. Pop, S. Sinha, K. E. Goodson, *Proc. IEEE* **94**, 1587–1601 (2006).
11. D. G. Cahill *et al.*, *Appl. Phys. Rev.* **1**, 011305 (2014).
12. Y. Gao, Y. Bando, *Nature* **415**, 599 (2002).
13. G. E. Begtrup *et al.*, *Phys. Rev. Lett.* **99**, 155901 (2007).
14. T. Brintlinger, Y. Qi, K. H. Baloch, D. Goldhaber-Gordon, J. Cumings, *Nano Lett.* **8**, 582–585 (2008).
15. M. Nonnenmacher, H. K. Wickramasinghe, *Appl. Phys. Lett.* **61**, 168 (1992).
16. L. Shi, S. Plyasunov, A. Bachtold, P. L. McEuen, A. Majumdar, *Appl. Phys. Lett.* **77**, 4295 (2000).
17. K. E. Goodson, M. Asheghi, *Microscale Thermophys. Eng.* **1**, 225 (1997).
18. N. N. Jarenwattananon *et al.*, *Nature* **502**, 537–540 (2013).
19. X. Wu, R. Hull, *Nanotechnology* **23**, 465707 (2012).
20. S. B. Vendelbo *et al.*, *Ultramicroscopy* **133**, 72–79 (2013).
21. H. Abe, M. Terauchi, R. Kuzuo, M. Tanaka, *J. Electron Microscop.* (Tokyo) **41**, 465 (1992).
22. G. Meyer, *Z. Phys.* **148**, 61–71 (1957).
23. P. Palanisamy, J. M. Howe, *J. Appl. Phys.* **110**, 024908 (2011).
24. Neglecting α_2 gives the simpler approximation $\Delta T = -2R/3\alpha_1$, but accounting for the temperature dependence of α is necessary because the resulting correction of $\sim 4\%$ per 100°C is larger than our sensitivity.
25. A. J. C. Wilson, *Proc. Phys. Soc.* **53**, 235–244 (1941).
26. Materials and methods are available as supplementary materials on Science Online.
27. E.-M. Steyskal *et al.*, *Phys. Rev. Lett.* **108**, 055504 (2012).
28. E. R. White, M. Mecklenburg, B. Shevitski, S. B. Singer, B. C. Regan, *Langmuir* **28**, 3695–3698 (2012).
29. R. F. Egerton, *Rep. Prog. Phys.* **72**, 016502 (2009).
30. O. L. Krivanek *et al.*, *Nature* **514**, 209–212 (2014).
31. K. A. Gschneidner, *Solid State Physics*, Frederick Seitz, David Turnbull, Eds. (Academic Press, 1964), vol. 16, pp. 275–426.

ACKNOWLEDGMENTS

This work has been supported by National Science Foundation award DMR-1206849 and in part by Function Accelerated nanoMaterial Engineering (FAME), one of six centers of Semiconductor Technology Advanced Research network (STARnet), a Semiconductor Research Corporation program

sponsored by the Microelectronics Advanced Research Corporation and Defense Advanced Research Projects Agency. Data presented in this article were acquired at the Center for Electron Microscopy and Microanalysis at the University of Southern California. Work at the Molecular Foundry was supported by the Office of Science, Office of Basic Energy Sciences, of the U.S. Department of Energy under contract DE-AC02-05CH11231.

SUPPLEMENTARY MATERIALS

www.sciencemag.org/content/347/6222/629/suppl/DC1
Materials and Methods
Table S1
Figs. S1 to S8
References (32, 33)

6 November 2014; accepted 12 January 2015
10.1126/science.aaa2433

EXOPLANET DYNAMICS

Asynchronous rotation of Earth-mass planets in the habitable zone of lower-mass stars

Jérémy Leconte,^{1,2,3*} Hanbo Wu,^{1,4} Kristen Menou,^{2,5} Norman Murray^{1,4}

Planets in the habitable zone of lower-mass stars are often assumed to be in a state of tidally synchronized rotation, which would considerably affect their putative habitability. Although thermal tides cause Venus to rotate retrogradely, simple scaling arguments tend to attribute this peculiarity to the massive Venusian atmosphere. Using a global climate model, we show that even a relatively thin atmosphere can drive terrestrial planets' rotation away from synchronicity. We derive a more realistic atmospheric tide model that predicts four asynchronous equilibrium spin states, two being stable, when the amplitude of the thermal tide exceeds a threshold that is met for habitable Earth-like planets with a 1-bar atmosphere around stars more massive than ~ 0.5 to 0.7 solar mass. Thus, many recently discovered terrestrial planets could exhibit asynchronous spin-orbit rotation, even with a thin atmosphere.

As we experience in our everyday life, atmospheric temperatures oscillate following the diurnal insolation cycle. This in turn creates periodic large-scale mass redistribution inside the atmosphere—the so-called thermal atmospheric tides. But as we all also have experienced, the hottest moment of the day is actually not when the Sun is directly overhead, but a few hours later. This is due to the thermal inertia of the ground and atmosphere that creates a delay between the solar heating and thermal response (driving mass redistribution), causing the whole atmospheric response to lag behind the Sun (1).

Because of this asymmetry in the atmospheric mass redistribution with respect to the subsolar

point, the gravitational pull exerted by the Sun on the atmosphere has a nonzero net torque that tends to accelerate or decelerate its rotation, depending on the direction of the solar motion (2, 3). Because the atmosphere and the surface are usually well coupled by friction in the atmospheric boundary layer, the angular momentum transferred from the orbit to the atmosphere is then transferred to the bulk of the planet, modifying its spin (4).

On Earth, this effect is negligible because we are too far away from the Sun, but the atmospheric torque due to thermal tides can be very powerful, as seen on Venus. Indeed, although tidal friction inside the planet is continuously trying to spin it down to a state of synchronous rotation, thermal tides are strong enough to drive the planet out of synchronicity and to force the slow retrograde rotation that we see today (2–6). Very simple scaling arguments predict that the amplitude of the thermal tide is proportional to the ratio of the atmospheric mean surface pressure over its scale height (1). Everything else being equal, one would thus expect the thermal tide to be ~ 50 times weaker if Venus had a less massive, cooler Earth-like atmosphere. Whether this scaling really holds and how massive the atmosphere

¹Canadian Institute for Theoretical Astrophysics, 60 St George Street, University of Toronto, Toronto, ON M5S3H8, Canada. ²Center for Planetary Sciences, Department of Physical and Environmental Sciences, University of Toronto Scarborough, Toronto, ON M1C 1A4, Canada. ³Laboratoire de Météorologie Dynamique, Institut Pierre Simon Laplace, 4 Place Jussieu, BP 99, 75252 Paris, France. ⁴Department of Physics, University of Toronto, 60 St George Street, Toronto, ON M5S 1A7, Canada. ⁵Department of Astronomy and Astrophysics, University of Toronto, Toronto, ON M5S 3H8, Canada.

*Corresponding author. E-mail: jleconte@cita.utoronto.ca

must be to affect the planetary rotation has not yet been determined.

These issues are of utmost importance as we now find many terrestrial planets in a situation similar to Venus. Because the habitable zone—the zone around a star inside which a planet can sustain surface liquid water—is closer around

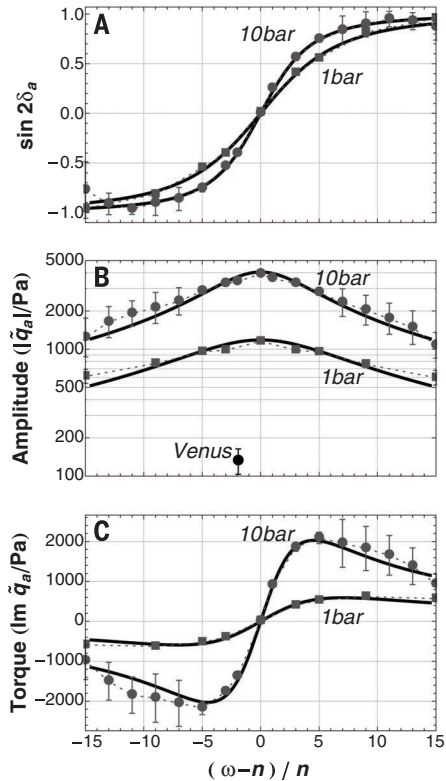


Fig. 1. Frequency dependence of the torque. (A) Sin of the lag angle ($\sin 2\delta_a$), (B) amplitude of the pressure bulge ($|\tilde{q}_a|$), and (C) torque [$\text{Im}(\tilde{q}_a)$] as a function of the forcing frequency [$(\omega - n)/n$] computed from the numerical atmospheric model (gray data points) and given by our analytical model (black curve). Results are shown for two pressures (squares, 1 bar; circles, 10 bar) in the 1366 W/m^2 case with an orbital period of 225 days. The error bars show the internal variability ($\pm 1\sigma$). The Venusian tide amplitude is shown in (B). Despite its simplicity, the analytical model fairly captures the frequency dependence of the thermal tide response.

Table 1. Characteristics of the thermal tide for various types of atmospheres. Numerical values of the amplitude of the atmospheric quadrupole (q_0) and intrinsic thermal frequency of the atmosphere (ω_0) derived from the global climate model.

Sets of simulations	Model output				
	$F(\text{W}\cdot\text{m}^{-2})$	p_s (bar)	q_0 (Pa)	ω_0 (s^{-1})	$2\pi/\omega_0$ (days)
Venus	2610	92	201	3.77×10^{-7}	193
Inner habitable zone	1366	1	1180	2.30×10^{-6}	32
		10	4050	1.46×10^{-6}	50
Outer habitable zone (N_2)	450	1	890	1.18×10^{-6}	62
		10	2960	7.17×10^{-7}	101
Outer habitable zone (CO_2)	450	10	2590	9.7×10^{-7}	70

lower-mass stars, planets in this region are often expected to be tidally synchronized with the orbit (7–15). This seems to create additional difficulties for keeping a habitable environment over the lifetime of the planet. In particular, the permanent night side can be an efficient cold-trap for water (13, 14), strongly destabilize the carbonate-silicate cycle (10, 11), and even cause atmospheric collapse in extreme cases (9, 15).

Here, we investigate whether or not thermal tides can drive terrestrial planets in the habitable zone out of synchronous rotation if a relatively thin atmosphere is present. Previous studies on Venus (2–6), and for exoplanets (16, 17), have shown that this reduces to the search for equilibrium rotation states for which the bodily torque (T_g) and the atmospheric torque (T_a) cancel each other and provide a restoring force against deviations from this equilibrium. In the circular case with zero obliquity, these torques are given by

$$T_a = -\frac{3}{2}K_a b_a(2\omega - 2n)$$

and

$$T_g = -\frac{3}{2}K_g b_g(2\omega - 2n) \quad (1)$$

where $K_a \equiv (3M_* R_p^3)/(5\bar{\rho} a^3)$; $K_g \equiv GM_*^2 R_p^5/a^6$; G is the universal gravitational constant; M_* is the mass of the star; R_p , ω , and $\bar{\rho}$ are the planet's radius, rotation rate, and mean density, respectively; and a and n are its orbital semimajor axis and mean motion, respectively (5, 6). $b_g(\sigma)$ characterizes the frequency- (σ) -dependent response of the body of the planet (its rheology), and $b_a(\sigma)$ characterizes that of the atmosphere. Unlike trapping in asynchronous spin-orbit resonances (for example, Mercury) (18), thermal tides do not need any eccentricity to drive a planet out of synchronous rotation. Although some general conclusions can be reached without a precise knowledge of these responses (5, 6, 16, 17), the biggest limitation in predicting the properties of equilibrium spin states lies in the uncertainties on the shape and amplitude of the atmospheric response [$b_a(\sigma)$]. In particular, the relation between the mass of the atmosphere and the strength of the thermal tide is key in quantifying whether asynchronousity is ubiquitous and remains unknown.

To tackle this issue, we use a generic global climate model (14, 19, 20), commonly used to model planets in the habitable zone of low-mass stars, to

empirically quantify the amplitude of torque induced by thermal tides for planets with various atmospheric masses (characterized by the surface pressure, p_s), compositions, and incoming stellar fluxes (F). Once p_s and F are chosen, we run the atmospheric model for several diurnal frequencies, $\sigma \equiv \omega - n$. Because of the thermal forcing, a surface pressure pattern lagging behind the substellar point forms (fig. S1). Once mean thermal equilibrium is reached, we compute the complex amplitude of the quadrupolar thermal tide (\tilde{q}_a) (21), as shown in Fig. 1, and the value of the torque is given by

$$\text{Eq. 1, where } b_a(2\omega - 2n) = -\sqrt{\frac{10}{3\pi}} \text{Im}[\tilde{q}_a(\omega - n)]$$

To test our framework, we applied our model to Earth and Venus, where our results meet existing constraints (fig. S2) (21). However—rather counterintuitively—for the same forcing frequency, the amplitude of the thermal tide in an Earth-like atmosphere of 1 bar is almost an order of magnitude stronger than on Venus (Fig. 1B). This difference is the result of the sunlight being almost completely scattered or absorbed before it reaches Venus's surface (21).

As discussed earlier, the lag and amplitude of thermal tides are closely related to the thermal inertia of the system. In fact, a careful analysis of the result of the climate model shows that the frequency dependence of the atmospheric response shown in Fig. 1 is fairly analogous to the thermal response of a radiating slab with a finite thermal inertia that is periodically heated. Therefore, to a very good approximation, we can write

$$\tilde{q}_a(\sigma) = -\frac{q_0}{1 + i\sigma/\omega_0}$$

where $i^2 = -1$, ω_0 is the inverse of the time scale needed for the system to reach thermal equilibrium, and q_0 is the amplitude of the quadrupole term of the pressure field at zero frequency (21). In theory, ω_0 can be estimated if the heat capacity of the system is known (21), but in practice, both ω_0 and q_0 are computed from the numerical model for a given atmosphere and are shown in Table 1 for limit cases. In the circular case with zero obliquity, the torque is expressed as

$$T_a(\omega - n, p_s, F) = \frac{3}{2}K_a q_0(p_s, F) \times \frac{(\omega - n)/\omega_0(p_s, F)}{1 + [(\omega - n)/\omega_0(p_s, F)]^2}$$

Although governed by different physics, the atmospheric torque follows the same law as the body torque for a viscoelastic sphere (with the opposite sign).

A first qualitative difference with previous works (3–5, 16, 17) is that we derive a very different functional form for the atmospheric torque. In particular, the function $f(\sigma) \equiv b_a(2\sigma)/b_g(2\sigma)$ (5) is not monotonic around potential equilibria when a realistic rheology is used. As seen in Fig. 2, for a constant- Q or an Andrade rheology, this results in the possible existence of up to five equilibria in the circular case, two of them being

unstable (21). The diversity of equilibria might be even richer in eccentric systems where these numbers could change (16, 17). The synchronous spin state is stable. Knowing that Venus, despite such a

rheology, did not end up synchronized tells us that a planet can avoid being trapped in such a stable synchronous state and constrains the history of the Venusian atmosphere (21).

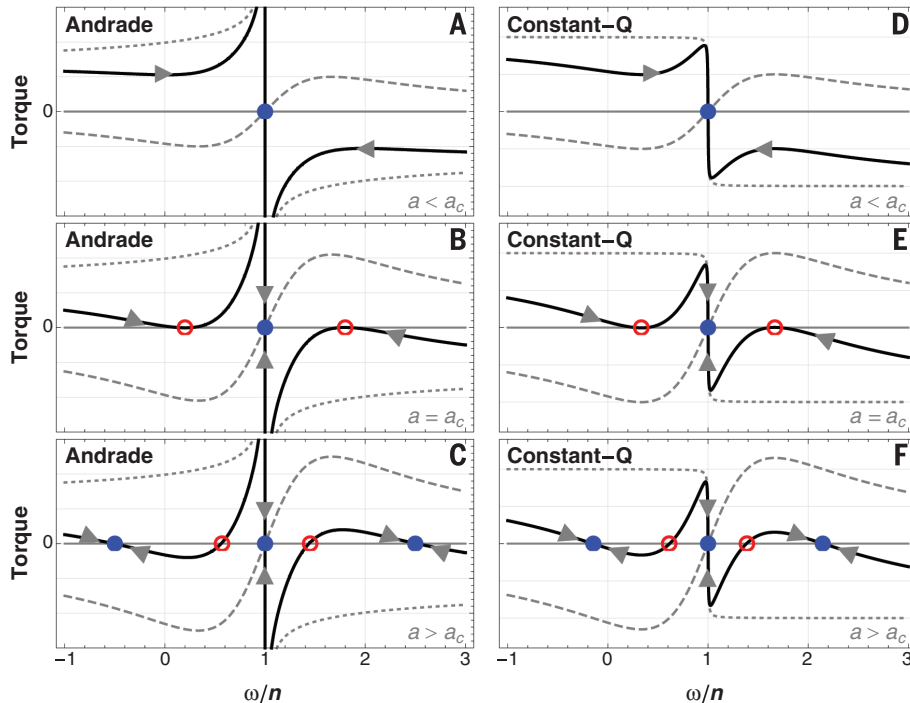
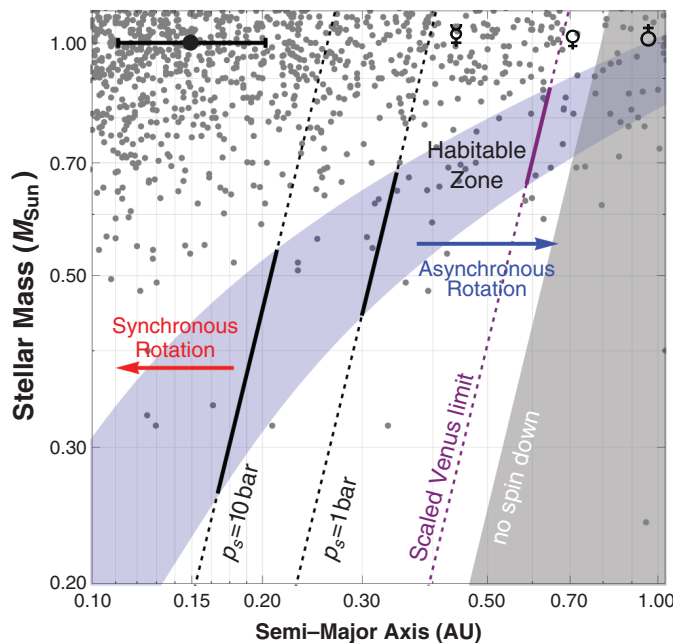


Fig. 2. Equilibrium spin states of the planet. Atmospheric (dashed), gravitational (dotted), and total (solid) torque as a function of spin rate for two tidal models, (A to C) Andrade and (D to F) Constant-Q. Arrows show the sense of spin evolution. (A) and (D) show weak atmospheric torque, only one equilibrium, and synchronous spin state exists (blue circle). (B) and (E) show the bifurcation point ($a = a_c$). In (C) and (F), the atmospheric torque is strong enough to generate four asynchronous equilibrium spin states, two being unstable (red open circles) and two being stable (blue circles; one is retrograde in the case shown). The synchronous spin state remains stable. The figure is to be compared with figure 6 of (24).

Fig. 3. Spin state of planets in the habitable zone. The blue region depicts the habitable zone (14, 25), and gray dots are detected and candidate exoplanets. Each solid black line marks the critical orbital distance (a_c) (Eq. 2) separating synchronous (left, red arrow) from asynchronous planets (right, blue arrow) for $p_s = 1$ and 10 bar (the extrapolation outside the habitable zone is shown with dotted lines). Objects in the gray area are not spun down by tides. The error bar illustrates how limits would shift when varying the dissipation inside the planet ($Q \sim 100$) (21) within an order of magnitude.



In addition, the number and location of equilibria undergo a bifurcation because asynchronous spin states exist only when the amplitude of the thermal tide reaches a threshold. Thus, our results reveal the existence of a critical distance a_c beyond which the planet can be asynchronous, which, using a constant- Q rheology, reads

$$a_c = \left(\frac{10\pi}{3}\right)^{1/6} \left(GM_* \bar{\rho} R_p^2 \frac{k_2}{q_0 Q}\right)^{1/3} \quad (2)$$

where k_2 is the Love number and Q is the tidal quality factor (21). Both a_c (Fig. 3) and the equilibrium asynchronicity $|\omega - n| = \omega_0[(a/a_c)^3 + \sqrt{(a/a_c)^6 - 1}]$ (fig. S3) can be computed for various cases by using Table 1. The corollary is that even without any spin-orbit trapping due to a permanent asymmetry of the mantle (triaxiality), planets on circular orbits for which atmospheric tides are too weak should be in exact spin-orbit resonance.

Our results provide a robust framework for the quantitative assessment of the efficiency of thermal tides for different atmospheric masses without having to rely on scaling arguments calibrated on Venus. This is crucial because Venus thermal tides turn out to be relatively weak (Fig. 1B). As can be seen in Fig. 3, Earth-like planets with a 1-bar atmosphere are expected to have a nonsynchronous rotation if they are in the habitable zone of stars more massive than ~ 0.5 to $0.7M_\odot$ (depending on their location in the habitable zone). This lower limit decreases to $\leq 0.3M_\odot$ for a 10-bar atmosphere. These limits are much less restrictive than the one obtained from our Venus model (Fig. 3, purple line). This realization required full atmospheric modeling.

Atmospheres as massive as 1 bar are a reasonable expectation value given existing models and solar system examples. This is especially true in the outer habitable zone, where planets are expected to build massive atmospheres with several bars of CO_2 (7). So, our results demonstrate that asynchronism mediated by thermal tides should affect an important fraction of planets in the habitable zone of lower-mass stars.

This has many implications. On one hand, the difficulties in sustaining a habitable climate far from the star due to the presence of a permanent cold, night side (9–15) may not be as severe as usually thought. On the other hand, the habitable zone has been recently shown to be more extended near the star for synchronous planets (12). For these objects, if the atmosphere is thick enough, the nonsynchronous rotation that should ensue may thus come to limit the extent of the habitable zone around lower-mass stars.

The thermal tide mechanism presented here does not only affect habitable-zone planets, so many other terrestrial bodies with substantial atmospheres could potentially have asynchronous rotations, depending on their orbital location (Fig. 3). With that in mind, observational methods

that can constrain the rotation rate of exoplanets (22, 23) become more valuable and could even be used to constrain their atmospheres.

REFERENCES AND NOTES

- S. Chapman, R. Lindzen, *Atmospheric Tides, Thermal and Gravitational* (Reidel, Dordrecht, 1970).
- T. Gold, S. Soter, *Icarus* **11**, 356–366 (1969).
- A. P. Ingersoll, A. R. Dobrovolskis, *Nature* **275**, 37–38 (1978).
- A. R. Dobrovolskis, A. P. Ingersoll, *Icarus* **41**, 1–17 (1980).
- A. C. Correia, J. Laskar, *Nature* **411**, 767–770 (2001).
- A. C. Correia, J. Laskar, *J. Geophys. Res. Planets* **108** (E11), 5123 (2003).
- J. F. Kasting, D. P. Whitmire, R. T. Reynolds, *Icarus* **101**, 108–128 (1993).
- R. Heller, J. Leconte, R. Barnes, *Astron. Astrophys.* **528**, A27 (2011).
- M. M. Joshi, R. M. Haberle, T. T. Reynolds, *Icarus* **101**, 108–128 (1993).
- E. S. Kite, E. Gaidos, M. Manga, *Astrophys. J.* **743**, 41 (2011).
- A. R. Edson, J. F. Kasting, D. Pollard, S. Lee, P. R. Bannon, *Astrobiology* **12**, 562–571 (2012).
- J. Yang, N. B. Cowan, D. S. Abbot, *Astrophys. J.* **771**, L45 (2013).
- K. Menou, *Astrophys. J.* **774**, 51 (2013).
- J. Leconte *et al.*, *Astron. Astrophys.* **554**, A69 (2013).
- K. Heng, P. Kopparla, *Astrophys. J.* **754**, 60 (2013).
- A. C. Correia, B. Levrard, J. Laskar, *Astron. Astrophys.* **488**, L63–L66 (2008).
- D. Cunha, A. C. Correia, J. Laskar, Spin evolution of Earth-sized exoplanets, including atmospheric tides and core-mantle friction. *Int. J. Astrobiol.*, 10.1017/S1473550414000226 (2014).
- V. V. Makarov, C. Berghea, M. Efroimsky, *Astrophys. J.* **761**, 83 (2012).
- F. Forget *et al.*, *Icarus* **222**, 81–99 (2013).
- J. Leconte, F. Forget, B. Charnay, R. Wordsworth, A. Pottier, *Nature* **504**, 268–271 (2013).
- Materials and methods are available as supplementary materials on Science Online.
- F. Selsis *et al.*, *Astron. Astrophys.* **555**, A51 (2013).
- I. A. G. Snellen *et al.*, *Nature* **509**, 63–65 (2014).
- A. C. M. Correia, J. Laskar, O. N. de Sury, *Icarus* **163**, 1–23 (2003).
- R. K. Kopparapu *et al.*, *Astrophys. J.* **765**, 131 (2013).

ACKNOWLEDGMENTS

J.L. thanks S. Lebonnois for providing the numerical outputs of the Venus model. The authors thank three anonymous referees for their insightful comments that substantially enhanced the manuscript. N.M. is supported in part by the Canada Research Chair program. This work was supported by grants from the Natural Sciences and Engineering Research Council of Canada to K.M. and N.M. J.L. is a Banting Fellow.

SUPPLEMENTARY MATERIAL

www.sciencemag.org/content/347/6222/632/suppl/DC1
Materials and Methods
Supplementary Text
Figs. S1 to S5
References (26–35)

14 July 2014; accepted 19 December 2014
10.1126/science.1258686

METALLURGY

Origin of dramatic oxygen solute strengthening effect in titanium

Qian Yu,^{1,2*} Liang Qi,^{1,3†} Tomohito Tsuru,³ Rachel Traylor,¹ David Rugg,⁴ J. W. Morris Jr.,¹ Mark Asta,¹ D. C. Chrzan,¹ Andrew M. Minor^{1,2§}

Structural alloys are often strengthened through the addition of solute atoms. However, given that solute atoms interact weakly with the elastic fields of screw dislocations, it has long been accepted that solution hardening is only marginally effective in materials with mobile screw dislocations. By using transmission electron microscopy and nanomechanical characterization, we report that the intense hardening effect of dilute oxygen solutes in pure α -Ti is due to the interaction between oxygen and the core of screw dislocations that mainly glide on prismatic planes. First-principles calculations reveal that distortion of the interstitial sites at the screw dislocation core creates a very strong but short-range repulsion for oxygen that is consistent with experimental observations. These results establish a highly effective mechanism for strengthening by interstitial solutes.

Solute atoms are intentionally added to pure metals so as to engineer their mechanical properties but may also be present because they are incorporated naturally during processing or service. The strengthening effect of such solutes ordinarily is due to their resistance to dislocation motion, which is conventionally attributed to the elastic interaction between the respective lattice strains of the solute atoms and the dislocations. In isotropic elasticity theory, however, a perfect screw dislocation results in only a shear stress field and does not interact with a solute atom that creates an isotropic vol-

ume change (1, 2). The interaction remains relatively weak even when anisotropic elasticity, anisotropic solute strain, and the “modulus effect” of the solute are taken into account. It follows that solution hardening is not ordinarily expected to be an effective hardening mechanism in metals with mobile screw dislocations.

First-principles calculations suggest that under appropriate conditions, there may be a strong, specific structural interaction between solute atoms and the dislocation core that is not captured by the continuum elastic field (3, 4). This raises the possibility that solution hardening may be effective when mobile screw dislocations are present.

The present work addresses solution hardening by small oxygen additions to hexagonally close-packed (HCP) α -Ti. This is a particularly attractive system for such studies both because of its technological importance and because of the dramatic hardening effect of small oxygen additions (5–9). We exploit recent advances in aberration-corrected transmission electron mi-

croscopy (TEM), in situ small-scale mechanical testing, three-dimensional (3D) dislocation analysis, and first-principles computational modeling to clarify solution-hardening in this system. The experimental evidence discussed below documents strong solution-hardening by oxygen, shows substantial solute pinning of screw dislocations, reveals the incorporation of oxygen atoms in the dislocation core, and illustrates interesting features of dislocation motion and reconfiguration in the presence of oxygen. The parallel first-principles calculations clarify the crystallographic source of the oxygen interaction with the screw dislocation core. The distortion of the interstitial sites at the dislocation core creates a very strong but short-range repulsion for oxygen atoms. As a result, dislocations can only move via a “mechanical shuffle” of the oxygen interstitial or by a local cross slip that creates immobile dislocation segments. Both mechanisms effectively pin the dislocation near the oxygen interstitial.

The experimental samples include nominally pure α -Ti with 0.1, 0.2, and 0.3 weight percent (wt %) O additions. All of the materials are solid solutions (their chemical compositions are shown in table S1), although a few precipitates were observed in the Ti-0.3 wt % O sample. Details of the sample preparation are provided in the supplementary materials. In hexagonal α -Ti, the primary mobile dislocations are believed to be $\langle a \rangle$ -type dislocations on the prismatic plane (1, 10), although perpendicular screw dislocations are also active. To characterize dislocations and image the oxygen in their immediate neighborhood, we used the Transmission Electron Aberration-Corrected Microscope (TEAM) 0.5 microscope, a double-aberration-corrected (scanning) TEM capable of producing images with 50-pm resolution (11). The types of the dislocations were first determined at low magnification by using standard $g\cdot b$ analysis. We found that a majority of the “near-edge” dislocations were not pure $\langle a \rangle$ -type; they demonstrated weak contrast under the [0002] reflection, indicating $\langle c \rangle$ components.

¹Department of Materials Science and Engineering, University of California, Berkeley, CA, USA. ²National Center for Electron Microscopy, Molecular Foundry, Lawrence Berkeley National Laboratory, Berkeley, CA, USA. ³Nuclear Science and Engineering Directorate, Japan Atomic Energy, Tokai-mura, Ibaraki, Japan. ⁴Rolls Royce, Derby DE24 8BJ, UK.

*These authors contributed equally to this work. †Present Address: Department of Materials Science and Engineering, Zhejiang University, China. ‡Present Address: Department of Materials Science and Engineering, University of Michigan, Ann Arbor, MI, USA.

§Corresponding author. E-mail: aminor@berkeley.edu



Asynchronous rotation of Earth-mass planets in the habitable zone of lower-mass stars

Jérémy Leconte *et al.*
Science **347**, 632 (2015);
DOI: 10.1126/science.1258686

This copy is for your personal, non-commercial use only.

If you wish to distribute this article to others, you can order high-quality copies for your colleagues, clients, or customers by [clicking here](#).

Permission to republish or repurpose articles or portions of articles can be obtained by following the guidelines [here](#).

The following resources related to this article are available online at www.sciencemag.org (this information is current as of April 10, 2016):

Updated information and services, including high-resolution figures, can be found in the online version of this article at:
</content/347/6222/632.full.html>

Supporting Online Material can be found at:
</content/suppl/2015/01/14/science.1258686.DC1.html>

This article has been **cited by** 2 articles hosted by HighWire Press; see:
</content/347/6222/632.full.html#related-urls>

This article appears in the following **subject collections**:
Planetary Science
/cgi/collection/planet_sci